https://doi.org/10.5194/egusphere-2025-6512
Preprint. Discussion started: 5 February 2026

Seasonal variation in aerosol chemistry drives new particle formation and CCN activity in a coastal city, China: insights from year-long online measurements in Fuzhou

Zihan Wang[1], Yishu Bian[2], Fuwang Zhang[3], Honglei Wang [1,2*], Wen Lin[2], Jun Hu[4], Tianliang Zhao[1], Lijian Shen[2,5], Zuxin Xie[2]

[1] Collaborative Innovation Center on Forecast and Evaluation of Meteorological Disasters (CIC–FEMD), China Meteorological Administration Aerosol–Cloud and Precipitation Key Laboratory, Nanjing University of Information Science and Technology, Nanjing 210044, China
[2] Fujian Key Laboratory of Severe Weather and Key Laboratory of Straits Severe Weather, China Meteorological Administration, Fuzhou 350001, China
[3] Fujian Provincial Environmental Monitoring Central Station, Fuzhou 350003, China
[4] Fujian Provincial Academy of Environmental Science, Fuzhou 350001, China
[5] Key Laboratory of Ecosystem Carbon Source and Sink, China Meteorological Administration (ECSS-CMA), Wuxi University, Wuxi 214105, China

Correspondence to: Honglei Wang (hongleiwang@nuist.edu.cn)

Abstract: New particle formation (NPF) is an important source of cloud condensation nuclei (CCN), which affects the global climate. Continuous observations in the coastal city of Fuzhou, conducted from June 2021 to May 2022, aimed to study NPF events and their impact on CCN. A total of 46 NPF events were identified, with a frequency of 12.7 %. The average formation rate (FR) and growth rate (GR) of particles were 3.94 ± 8.26 $cm^{-3}·s^{-1}$ and 5.20 ± 1.78 $nm·h^{-1}$. The NPF events showed evident seasonal variation: spring (27.17 %), fall (9.89 %), winter (8.89 %), and summer (4.35 %). Spring NPF events were characterized by high FR (5.56 $cm^{-3}·s^{-1}$) and suppressed growth processes, while summer exhibited the highest GR among all seasons (peak at 11.68 $nm·h^{-1}$). The influence of NPF on the chemical composition of $PM_{2.5}$ and CCN also showed seasonal differences. In spring and summer, NPF generated substantial amounts of sulfate and nitrate, resulting in stronger particle hygroscopicity (> 0.1). In fall and winter, higher concentrations of black carbon (BC) and primary organic carbon (POC) led to weaker κ (0.09). The enhancement effect of NPF on CCN was most significant in summer (E_N_{CCN} = 1.64), accompanied by CCN growth. In spring, the high condensation sink (CS) suppressed growth, leading to an insignificant CCN enhancement effect. In fall and winter, NPF-induced CCN enhancement mainly

https://doi.org/10.5194/egusphere-2025-6512
Preprint. Discussion started: 5 February 2026

occurred 3–5 hours after the event, with increases ranging from 13 % to 65 %, particularly notable at high supersaturation levels (0.8–1.0 % SS).

1 Introduction

New particle formation (NPF) is a complex process in which gaseous precursors in the atmosphere nucleate and condense to form new particles, which subsequently grow through condensation, coagulation, and other processes. NPF contributes over 50 % of the global cloud condensation nuclei (CCN), significantly influencing cloud albedo, structure, lifetime, and solar radiation reaching the Earth's surface (Tröstl et al., 2016; Yao et al., 2018). Additionally, efficient nucleation and explosive growth of particles are important sources of haze formation in urban atmospheres, impacting air quality and public health (Kulmala et al., 2021).

Although its frequency may vary with season and location, NPF events fundamentally represent competition between aerosol particle sources and sinks. Current research indicates that secondary particle formation is driven by the photochemical oxidation of atmospheric gases. Sulfuric acid and highly oxidized molecules can act as nucleation precursors (Fan et al., 2018; Zaveri et al., 2022). Furthermore, ions may also play a role in particle nucleation, though their significance remains debated (Hirsikko et al., 2011; Kirkby et al., 2016). Pre-existing aerosol particles act as a sink for these precursors, small clusters, and newly formed particles, thereby suppressing NPF occurrence (McMurry and Friedlander, 1979). However, frequent NPF events also occur in heavily polluted cities (Sun et al., 2015; Yao et al., 2018). Therefore, the mechanisms governing NPF generation and growth under different atmospheric conditions are still under investigation.

NPF events can be described by the formation rate (FR) of nucleation-mode particles and the growth rate (GR) of newly formed particles (Kulmala et al., 2012). The formation rate of 3 nm particles in the boundary layer typically ranges from 0.01 to 10 $cm^{-3}s^{-1}$, while the typical growth rate in mid-latitudes ranges from 1 to 20 nm h^{-1} (Kulmala et al., 2004). Yli-Juuti et al. (2011) reported typical growth rates of 1.8–10.7 nm h^{-1} for 1.5–20 nm particles. Additionally, NPF occurrence is constrained by atmospheric temperature and humidity (Yu et al., 2017; Yue and Hamill, 1979), as well as the atmospheric environment and chemical composition (Chen et al., 2012; Kawana et al., 2022). Previous studies have

https://doi.org/10.5194/egusphere-2025-6512
Preprint. Discussion started: 5 February 2026

shown that NPF is enhanced in the presence of sulfuric acid, alkaline substances, organic acids, and ions (Wang et al., 2011), but suppressed in the presence of nitrogen oxides (NO_x) (Wildt et al., 2014), indicating significant synergistic effects in chemically complex mixtures (Guo et al., 2014)

Aerosol chemical composition also influences aerosol hygroscopicity, altering its critical diameter and thereby affecting CCN activation and cloud formation (Petters and Kreidenweis, 2007; Williamson et al., 2019; Xu et al., 2020). Under various atmospheric conditions, aerosols have positive feedback on CCN number concentration (N_{CCN}) (Fan et al., 2018). N_{CCN} typically shows a significant increase following NPF events (Kuwata et al., 2008; Yue et al., 2011). Kuwata et al. (2008) observed a clear increase in N_{CCN} at different supersaturation levels after NPF events on Jeju Island, South Korea. Research in Beijing indicated that NPF events could increase local N_{CCN} by 0.4–6 times (Yue et al., 2011). However, some studies suggest that an increase in hydrophobic organic components during subsequent particle growth may inhibit CCN generation. Therefore, understanding the role of different components during particle growth is crucial for assessing their subsequent climate effects.

Although NPF research in China is widespread, most studies focus on reporting occurrence frequencies, formation, and growth rates, or are limited to discussing nucleation mechanisms. For instance, NPF event frequencies at sites like Shangdianzi, Mount Tai, and Lin'an in eastern China range from 15 % to 29 % (Shen et al., 2018). Frequencies in Beijing, Jinan, and Shanghai are approximately 30 %, 40 %, and 21 %, respectively (Jayaratne et al., 2017; Lv et al., 2018; Xiao et al., 2015). However, a deeper understanding of its mechanisms, especially the quantification of its ultimate climate effects, remains a challenge and frontier in current research (Cai et al., 2018; Kulmala et al., 2021; Rose et al., 2017; Xiao et al., 2015; Yao et al., 2018). Given that Fuzhou is a rapidly developing southeastern coastal city with unique sea-land breeze conditions, a high-temperature and high-humidity environment, and complex pollution emission characteristics, it may have unique NPF mechanisms. Therefore, this study conducted a one-year comprehensive observation in Fuzhou from June 2021 to May 2022, providing new insights and data support for understanding the climate effects of NPF under China's complex atmospheric environment.

https://doi.org/10.5194/egusphere-2025-6512
Preprint. Discussion started: 5 February 2026

2 Data and Methods

2.1 Observation site

Observation data for this study were collected from June 1, 2021, to May 30, 2022, at the Fujian Provincial Environmental Monitoring Center Station and the Fuzhou Meteorological Bureau Station. Comprehensive atmospheric environmental observations were conducted at the Fujian Provincial Environmental Monitoring Center Station (26.11 °N, 119.30 °E, altitude around 65 m) and the Fuzhou Meteorological Bureau Station (26.05 °N, 119.26 °E, altitude around 18 m). Both stations are located within Fuzhou's urban area, approximately 8 km apart horizontally. The Fujian Provincial Environmental Monitoring Center Station is situated in Gulou District, the central urban area of Fuzhou, surrounded primarily by commercial, residential, and transportation land, representing areas heavily influenced by intense human activities. The Fuzhou Meteorological Bureau Station is located in Cangshan District, southern Fuzhou, approximately 1.5 km east of the Min River. Fuzhou is situated at the Min River estuary and along the East China Sea coast, characterized mainly by plains (average altitude 10-30 m) and a typical East Asian monsoon climate, significantly influenced by sea-land breeze circulation and marine air masses (Hu et al., 2024).

2.2 Measurement and instrumentation

A CCN counter (CCN-100; DMT, USA) equipped with a continuous flow of 500 cm^3/min and a thermal gradient was used to measure CCN concentrations at five supersaturation (SS) levels. To maintain counting accuracy, the instrument was regularly calibrated for T gradient, flow rate, pressure, SS, and OPC using standard ammonium sulfate according to the method by Rose et al. (2008). Additionally, zero-point determination was performed before and after each observation to minimize instrumental error. During observations, the measurement interval for each SS level was 10 minutes, and a few minutes were required to stabilize after switching SS levels. Therefore, CCN data collected before reaching stable SS were excluded from subsequent analysis.

An online organic carbon/elemental carbon analyzer (Sunset Laboratory semicontinuous OC/EC analyzer, Model-4, Sunset Laboratory Inc., USA) was used to determine organic carbon (OC) and

https://doi.org/10.5194/egusphere-2025-6512
Preprint. Discussion started: 5 February 2026

elemental carbon (EC) content in atmospheric particulate matter samples. Details of instrument operation can be found in (Chang et al., 2017).

A Wide-Range Particle Spectrometer (WPS-1000, MSP) measured aerosol number concentrations (10-350 nm) with a time resolution of 5 minutes across 96 channels. Instrument details and principles are described in (Wang et al., 2014).

Black carbon (BC) mass concentration was measured using an Aethalometer (AE-33, Magee) with a time resolution of 1 second, as detailed in (Kirchstetter et al., 2004). BC mass concentration data from the 880 nm wavelength (channel 6) were used.

An online particle chromatograph (A model online analyzer for Aerosols and Gases) continuously monitored mass concentrations of soluble aerosol ionic components (SO_4^{2-}, NO_3^-, NH_4^+, Na^+, K^+, Ca^{2+}, Cl^-) and trace gases (NH_3, HNO_2, HNO_3, HCl, SO_2). Sampling, operation, and internal calibration methods for the MARGA followed Du et al. (2011).

Meteorological data (including wind speed (WS), wind direction (WD), temperature (T), relative humidity (RH), and precipitation) with a time resolution of 1 hour were obtained from the Fuzhou Olympic Sports Center Meteorological Station. Data on conventional air pollutants (O_3, CO, NO_2, $PM_{2.5}$, and PM_{10}) were sourced from the China National Environmental Monitoring Centre's real-time urban air quality release platform (https://quotsoft.net/air/).

2.3 Analysis methods

The growth rate (GR) of new particles was calculated following (Kulmala et al., 2012):

$$GR = \frac{\Delta D_m}{\Delta t} \quad (1)$$

where D_m is the median diameter of the nucleation mode particles, obtained by fitting a log-normal distribution to the particle number size distribution.

The formation rate (FR) of new particles was calculated following Kulmala et al. (2012):

$$FR = \frac{dN_{nuc}}{dt} + CoagS_{nuc} \cdot N_{nuc_{dp}} + \frac{GR}{\Delta dp} + S_{losses} - losses \quad (2)$$

where N_{nuc} is the number concentration of nucleation-mode particles. Following the definition by Kulmala et al. (2012), the nucleation-mode size range in this study was also limited to below 25 nm.

https://doi.org/10.5194/egusphere-2025-6512
Preprint. Discussion started: 5 February 2026

$CoagS_{nuc}$ is the coagulation sink for nucleation-mode particles, and GR is the growth rate. The last two terms are generally negligible (Maso et al., 2005).

The condensation sink (CS) reflects the rate at which condensable vapor molecules condense onto the surface of pre-existing atmospheric particles and was calculated as follows (Kulmala et al., 2012):

$$FR = \frac{dN_{nuc}}{dt} + CoagS_{nuc} \cdot N_{nuc_{dp}} + \frac{GR}{\Delta dp} + S_{losses} - losses \quad (2)$$

where D is the diffusion coefficient of the vapor (typically assumed to be sulfuric acid), N_i is the number concentration of particles in a given size bin, and β_M is a correction factor.

The coagulation sink (CoagS) reflects the ability and rate of pre-existing atmospheric particles to remove newly formed nucleation particles via coagulation. For particles of size i, the coagulation sink can be expressed as:

$$CoagS_i = \sum_j K_{ij} N_j \quad (4)$$

where N_j is the number concentration of particles in size bin j, and K_{ij} is the Brownian coagulation coefficient between particles of size j and i.

The concentration of condensable vapor (C) was calculated using:

$$C = A \times \frac{dDp}{dt} \quad (5)$$

where Dp is the particle diameter, and A is a constant (1.37×10^{-7} $h\cdot cm^{-3}\cdot nm^{-1}$).

The hygroscopicity parameter (κ) was calculated based on the volume fraction of chemical components using a simple mixing rule (assuming internal mixture):

$$\kappa = \sum_i \varepsilon_i \kappa_i \quad (6)$$

where κ_i and ε_i represent the hygroscopicity parameter and volume fraction of component i in the mixture, respectively, and i denotes the number of components. This study calculated κ using the overall chemical composition of particles (mainly including organics, $(NH_4)_2SO_4$, and NH_4NO_3). Based on laboratory measurements (Petters and Kreidenweis, 2007), the κ values for pure $(NH_4)_2SO_4$ and NH_4NO_3 are 0.61 and 0.67, respectively.

The concentrations of secondary organic carbon (SOC) and primary organic carbon (POC) were estimated following (Wu and Yu, 2016):

$$POC = (OC/EC)_{min} \times EC \quad (7)$$

https://doi.org/10.5194/egusphere-2025-6512
Preprint. Discussion started: 5 February 2026

$$SOC = OC_{total} - (OC/EC)_{pri} \times EC \quad (8)$$

where OC_{total} is the measured OC, $(OC/EC)_{min}$ is the minimum (OC/EC) ratio during the observation period, POC is primary organic carbon, and SOC is secondary organic carbon.

The enhancement effect on cloud condensation nuclei number concentration (E_N_{CCN}) was defined as the ratio of CCN number concentration after the NPF event to that before the event (Ren et al., 2021):

$$E\_N_{CCN} = N_{CCN,\,after} / N_{CCN,\,prior} \quad (9)$$

where $N_{CCN,\,after}$, is the average N_{CCN} during the period from the start to the end of the NPF event, and $N_{CCN,\,prior}$, is the average N_{CCN} during the 2 hours before the NPF event.

2.4 Identification of NPF events

NPF events were identified based on criteria from Kulmala et al. (2012): (1) significant increase in nucleation-mode number concentration (N_{nuc}) (diameter 10–25 nm); (2) formation of a new mode lasting several hours; (3) growth of the newly formed mode over several hours. Additional criteria for NPF identification included: low pre-existing particle number concentration, a clear "banana-shaped" evolution in particle number concentration over time and size, and exclusion of interference from pre-existing particles (especially in urban environments) (Heintzenberg et al., 2007). In this study, a day was defined as an effective NPF day if the nucleation-mode (10–25 nm) particle number concentration increased continuously for at least 2 h from its initial value to its maximum and showed clear growth to larger sizes (e.g., 12–50 nm) over several hours (Fig. 1). Other days were defined as non-NPF days (Leng et al., 2014).

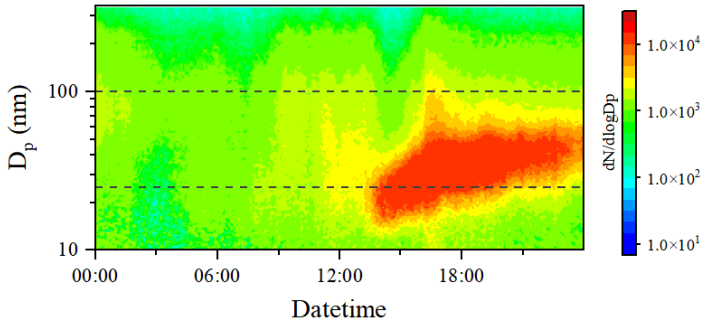

Fig. 1 An example NPF event observed on 21 April 2022.

https://doi.org/10.5194/egusphere-2025-6512
Preprint. Discussion started: 5 February 2026

3 Results and Discussion

3.1 Overall characteristics of NPF occurrence

NPF events in Fuzhou exhibited a distinct seasonal preference. As shown in Fig. 2a, spring was the season with the highest NPF frequency (27.17 %), while summer had the lowest (4.35 %). Fall (9.89 %) and winter (8.89 %) showed intermediate to low frequencies. NPF events mainly occurred between 9:00 and 12:00.

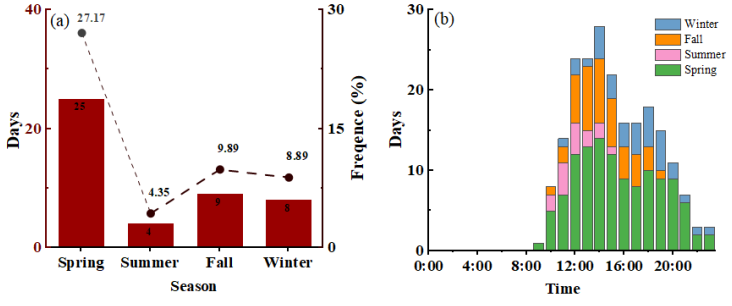

Fig. 2 The occurrence frequency and diurnal distribution of NPF events.

NPF events led to significant increases in nucleation-mode (N_{nuc}) and Aitken-mode (N_{ait}) particle number concentrations (Fig. S1). Spring showed the highest increase in N_{nuc} (196.7 %), while fall showed the highest increase in N_{ait} (70.5 %), indicating differences in new particle formation and subsequent growth across seasons.

NPF days typically corresponded to a lower background of $PM_{2.5}$ and PM_{10} (Fig. S2), indicating that NPF occurred in relatively clean atmospheres with a weak condensation sink. In spring, summer, and winter, POC on NPF days were lower than on non-NPF days, corroborating this point. Meanwhile, in spring, summer, and fall, SOC was higher on NPF days, suggesting that secondary organic vapors may actively participate in particle formation and growth.

Pollution levels were relatively higher in spring and winter, with SO_2 on NPF days exceeding those on non-NPF days (spring: 0.64 vs. 0.53 $\mu g \cdot m^{-3}$; winter: 0.88 vs. 0.76 $\mu g \cdot m^{-3}$; Fig. S3). NPF days in summer and fall presented a cleaner background environment, with NH_3 and NO_2 significantly lower than on non-NPF days. Regarding secondary inorganic ions, sulfate, nitrate, and ammonium on NPF days were lower than on non-NPF days in summer, fall, and winter (Fig. S4). In spring, secondary inorganic ions

https://doi.org/10.5194/egusphere-2025-6512
Preprint. Discussion started: 5 February 2026

on NPF days were comparable to non-NPF days, suggesting that abundant precursors in spring might overcome the inhibitory effect of a high condensation sink, thereby promoting NPF events.

The average particle hygroscopicity parameter (κ) on NPF days was significantly lower than on non-NPF days across all seasons (Fig. S5). Despite reduced hygroscopicity, NPF events effectively increased atmospheric CCN number concentrations. At supersaturations above 0.4 %, N_{CCN} on NPF days was higher than on non-NPF days in all seasons except spring, with the most significant increases observed in winter and fall (Fig. S6).

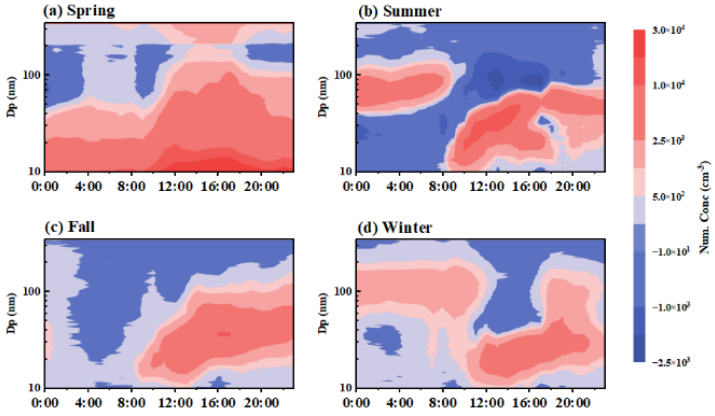

Fig. 3 The differences in particle number size distributions between NPF days and non-NPF days for each season.

Figure. 3a shows that in spring, particle number concentrations in the 10–20 nm range are generally elevated. NPF typically occurs from 9:00 to 20:00, with the peak concentration of 10–15 nm particles reaching 29,498 cm^{-3}. Concurrently, the concentration of particles >20 nm also increases significantly, some of which can grow beyond 100 nm. The aerosol size distributions on NPF days in summer, fall, and winter all exhibit an NPF process pattern similar to that shown in Fig. 1(Figure 3b-d), typically occurring in 09:00–20:00. During summer NPF events, the maximum particle number concentration reaches approximately 11,410 cm^{-3}, with particles growing up to around 50 nm. In fall and winter, the peak particle number concentrations are lower than in summer (fall and winter, 10110 and 5276 cm^{-3}), indicating weaker NPF intensity, and the maximum particle growth can extend up to 100 nm in these seasons.

https://doi.org/10.5194/egusphere-2025-6512
Preprint. Discussion started: 5 February 2026

3.2 Evolution characteristics and key parameters of NPF events

Spring NPF events had the highest formation rate (FR=7.13 $cm^{-3}\cdot s^{-1}$) and the highest condensation sink (CS=4.1×10^{-2} s^{-1}) among all seasons (Table 1). Before NPF events (-4 to 0 h), N_{nuc} increased from 5425 to 7701 cm^{-3}, peaking at 1 h (8840 cm^{-3}), then gradually declining. This trend was consistent with changes in the FR (Fig. 4a). FR rose sharply to 6.31 $cm^{-3}\cdot s^{-1}$ at the onset of NPF (0 h) and peaked at 7.21 $cm^{-3}\cdot s^{-1}$ at 1 h, demonstrating strong new particle formation capability. However, intense competition under a high CS background significantly suppressed subsequent growth. The growth rate (GR) exhibited large fluctuations, reverting to a negative value at 3 h after an initial peak. N_{ait} increased by only 32 % from 0 h to its peak at 2 h, much lower than in other seasons. Spring NPF events were characterized by strong formation but suppressed growth under high CS.

Table 1. Seasonal variations in key parameters of NPF events: particle growth rate (GR), formation rate (FR), coagulation sink (CoagS), condensable vapor concentration (C) and its production rate (Q), condensation sink (CS), and hygroscopicity parameter (κ).

Average	FR ($m^{-3}\cdot s^{-1}$)	GR ($nm\cdot h^{-1}$)	CS ($\times 10^{-2}\cdot s^{-1}$)	CoagS ($\times 10^{-4}\ s^{-1}$)	C ($\times 10^{7}\ cm^{-3}$)	κ
Total	3.94	5.20	3.1	3.9	16.7	0.12
Spring	7.13	3.69	4.1	5.2	20.1	0.19
Summer	0.40	4.20	1.8	2.0	10.9	0.1
Fall	0.28	2.35	2.0	1.8	9.5	0.09
Winter	0.23	1.87	2.1	1.9	4.7	0.08

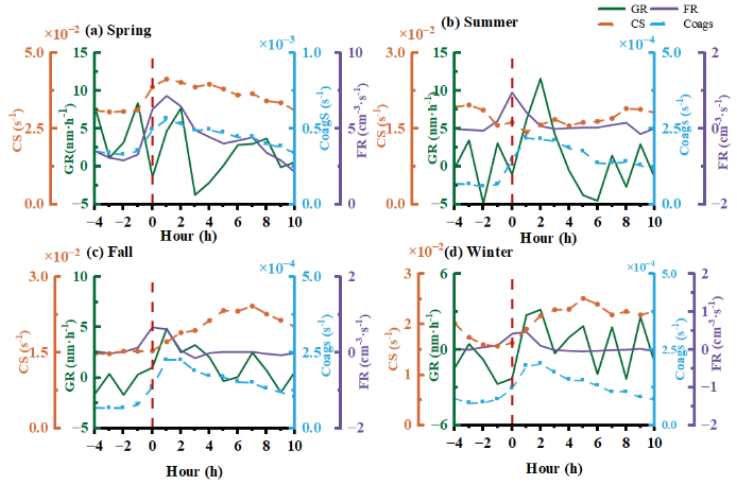

Fig. 4 Key NPF parameters: growth rate (GR), formation rate (FR), condensation sink (CS), and coagulation sink (CoagS) for seasons.

https://doi.org/10.5194/egusphere-2025-6512
Preprint. Discussion started: 5 February 2026

Despite the low average FR (0.40 $cm^{-3} \cdot s^{-1}$, Table 1), summer exhibited the highest average GR (4.20 $nm \cdot h^{-1}$), and the lowest average CS (1.8×10^{-2} s^{-1}). In summer NPF events (Fig. 4b), N_{nuc} peaked at 1 h (3459 cm^{-3}). FR relatively high from 0–2 h (0.97-0.44 $cm^{-3} \cdot s^{-1}$). The most prominent feature of summer was the high growth efficiency (GR) under the lowest CS, with a maximum peak of 11.68 $nm \cdot h^{-1}$ at 2 h. After NPF onset in summer, N_{ait} peaked at 3 h (6461.6 cm^{-3}), with the highest increase of 202.91 %. This indicates that the growth process of new particles in summer NPF events was far stronger than particle formation.

Winter had the lowest average FR (0.23 $cm^{-3} \cdot s^{-1}$) and GR (1.87 $nm \cdot h^{-1}$, Table 1). Winter NPF events were characterized by a low FR and delayed growth under a low condensation sink (CS), as shown in Table 1. In Fig.4d, the FR peak observed at 0 h (0.43 $cm^{-3} \cdot s^{-1}$) was the lowest among all seasons, indicating weak nucleation. In contrast, the growth rate (GR) displayed a distinct multi-peak pattern, with an initial peak at 2 h (3.20 $nm \cdot h^{-1}$) and subsequent peaks occurring between 5 and 9 h, suggesting that different mechanisms may have driven particle growth at different stages. Correspondingly, N_{ait} reached a maximum at 3 h (4794.2 cm^{-3}), which was the lowest seasonal peak (Fig. S7). Nevertheless, N_{ait} remained at relatively high levels (4500–4800 cm^{-3}) over an extended period from 2 to 6 h, reflecting sustained particle growth throughout the event.

Fall presented transitional characteristics, with average FR (0.28 $cm^{-3} \cdot s^{-1}$) and GR (2.35 $nm \cdot h^{-1}$) higher than winter but lower than spring and summer (Table 1). Fall NPF process parameters showed transitional characteristics between summer and winter, generally similar to winter (Fig. 4c). Its FR peak (0.68 $cm^{-3} \cdot s^{-1}$) and GR peak (4.90 $nm \cdot h^{-1}$) were higher than winter but much lower than spring and summer. The increase in N_{ait} after NPF onset was 165 %, significantly stronger than in winter (Fig. S7). The N_{ait} peak (6240.9 cm^{-3}) occurred latest (4 h) and remained above 5600 cm^{-3} from 5–7 h, higher than winter.

Aerosol hygroscopicity (κ) during NPF events also exhibited notable seasonal contrasts (Fig. S8). In winter, κ decreased sharply after event onset (from 0.12 to 0.02), rebounded after 6 h (0.06), and continued rising until 10 h (0.10), a pattern distinct from the other three seasons, where κ generally increased following NPF events.

In spring, κ varied modestly (0.14–0.19), rising from 0.15 to 0.19 within the first hour and stabilizing near 0.16 thereafter. Summer showed the most pronounced increase, from 0.12 before the event to 0.31

https://doi.org/10.5194/egusphere-2025-6512
Preprint. Discussion started: 5 February 2026

at 4 h post-onset, with a secondary peak (0.28) observed 8 h after the event ended. In fall, κ began increasing from -2 h, peaked at 0 h (0.094–0.10), then gradually declined, with a slight rebound between 4–6 h (0.08–0.11).

Overall, κ displayed both increases (in spring and summer) and decreases (in fall and winter) during NPF events, reflecting seasonal differences in aerosol chemical composition.

3.3 Influence of chemical composition on NPF events

Spring NPF days were characterized by the highest CS (4.1×10^{-2} s^{-1}) and were predominantly influenced by secondary pollution. Before NPF events, gaseous SO_2 and NH_3 increased from 0.47 and 5.01 $\mu g \cdot m^{-3}$ to 0.89 and 5.95 $\mu g \cdot m^{-3}$, respectively (Fig. 5a). Two hours after NPF onset, their concentrations began to decline continuously, indicating substantial consumption. Mass concentrations of secondary inorganic salts (SO_4^{2-} and NO_3^-) fluctuated between 4.5–4.8 $\mu g \cdot m^{-3}$ and 4–6 $\mu g \cdot m^{-3}$, respectively. Although NO_3^- showed minor fluctuations, it remained at relatively high levels (Fig. 6a). NPF events occurred under stable high-pressure systems (average pressure 1015 hPa), accompanied by systematic warming (from 18.9 to 23.2 °C) and drying (RH, 76 to 60 %) (Fig. S9a), favoring accelerated photochemical reactions and gas-particle conversion of semi-volatile gases (Chen et al., 2023). Wind speeds were generally low (<1.9 $m \cdot s^{-1}$), and the atmospheric stratification was stable. After NPF onset, O_3 increased significantly (from 81.1 to 98.8 $\mu g \cdot m^{-3}$; Fig. S11a), indicating enhanced atmospheric oxidizability. Precursor gases (SO_2 and NO_2) were oxidized via photochemistry to form NO_3^- and SO_4^{2-}, promoting the generation of secondary inorganic salts and secondary aerosols, including secondary organic aerosol (Fig. S10a). Abundant secondary inorganic salts generated in the early stages could act as condensation nuclei. Despite the high CS background, spring had high-frequency and high-FR NPF events, primarily attributed to higher precursor gas and strong photochemistry. However, high CS competed for condensable vapors and scavenged newly formed particles, suppressing the growth stage of new particles. Additionally, during the NPF stage, high concentrations of sulfate (4.4–5.0 $\mu g \cdot m^{-3}$), nitrate (4.6–5.3 $\mu g \cdot m^{-3}$), and ammonium (2.6–3.0 $\mu g \cdot m^{-3}$) were observed. The coexistence of these highly hygroscopic ionic components resulted in the highest κ (0.19) (Jokinen et al., 2018).

https://doi.org/10.5194/egusphere-2025-6512
Preprint. Discussion started: 5 February 2026

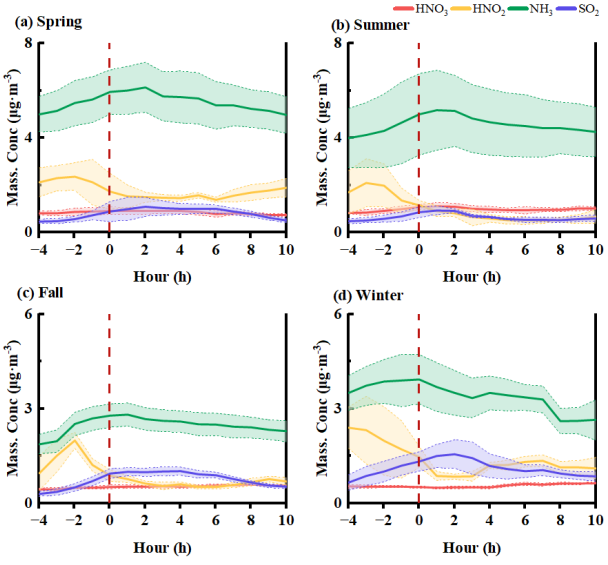

296

297 **Fig. 5 The evolution of relevant trace gases for different seasons.**

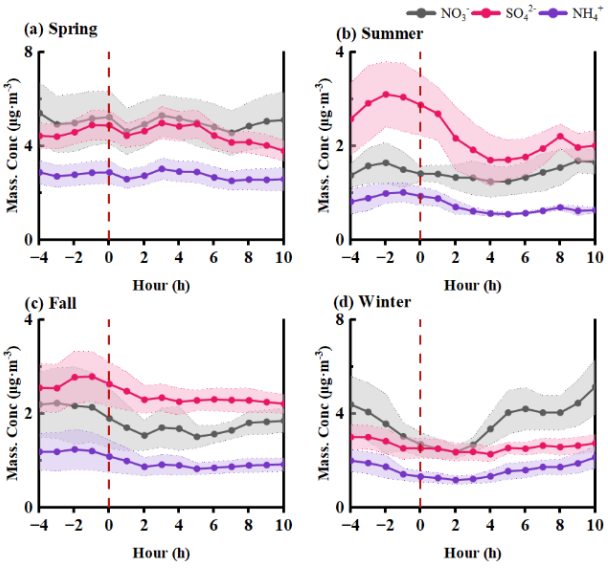

298

299 **Fig. 6 The evolution of ion composition for seasons.**

300 CS in summer, fall, and winter were relatively low (around 2.0×10^{-2} s^{-1}), indicating fewer surfaces

301 available for condensation in the atmosphere.

https://doi.org/10.5194/egusphere-2025-6512
Preprint. Discussion started: 5 February 2026

Summer NPF days had the lowest CS (1.8×10^{-2} s^{-1}) and a clean atmospheric environment. NPF events occurred under a high-temperature environment (>32 °C) (Fig. S9b), which inhibits nucleation (Yu et al., 2017). At NPF onset, wind speed surged (2.37 $m\cdot s^{-1}$) and shifted from southerly to westerly. This might be related to sea breeze development, diluting the gaseous precursors (Fig. 5b) and pollutants (Fig. S1b), especially SO_2, which decreased overall from 0.51 to 0.94 $\mu g\cdot m^{-3}$. Therefore, despite favorable conditions of low CS and ample sunlight, summer NPF frequency and formation rate were low, and atmospheric oxidizability was weak (O_3: 48.5–52.7 $\mu g\cdot m^{-3}$; Fig. S11b). After NPF onset, average wind speeds remained relatively high (>1.7 $m\cdot s^{-1}$). As ozone continued to rise (0–6 h), secondary ions (NO_3^-, SO_4^{2-}) and SOC increased (Fig. 6b and Fig. Sb). These efficiently condensed onto particle surfaces under a low CS background, achieving extremely high growth efficiency (GR peak of 11.59 $nm\cdot h^{-1}$). However, the κ in summer was intermediate between spring and winter.

Before Fall NPF events, SO_2 and NH_3 increased from 0.36 and 1.99 $\mu g\cdot m^{-3}$ to 2.83 and 2.83 $\mu g\cdot m^{-3}$, respectively (Fig. 5c). The lower temperature (around 22 °C) and high humidity (RH >71 %) environment (Fig. S9c) favored the combination of sulfuric acid molecules, promoting nucleation (Lehtipalo et al., 2018; Tröstl et al., 2016; Yue and Hamill, 1979). After NPF onset, although atmospheric oxidizability increased continuously (O_3 from 36 to 94 $\mu g\cdot m^{-3}$), it was short-lived. After 4 h, as O_3 gradually decreased and primary emissions increased, pollutant accumulation occurred, and BC and POC rebounded (Fig. S10c). The contribution of primary emissions (e.g., BC, POC) to aerosols was significantly enhanced, and overall hygroscopicity (κ=0.09) was low.

Winter NPF events were also preceded by an accumulation of gaseous precursors (Fig. 5d). However, elevated emissions from sources such as heating led to high BC and POC during the initial NPF stage (1.86 and 1.02 $\mu g\cdot m^{-3}$ at -4 h, Fig. S10d). These abundant primary particles strongly suppressed new particle formation via intense coagulation scavenging, resulting in persistently low formation rates (FR $\leqslant$0.47 $cm^{-3}\cdot s^{-1}$). Photochemical activity was limited under low winter temperatures (Fig. S9d). As temperatures continued to drop later in the event (after 6 h), condensation-driven conversion of gaseous precursors to particles increased (Jokinen et al., 2018). This was particularly evident in the rapid formation of particulate ammonium nitrate from HNO_3 and NH_3 between 6–10 h (Fig. 5d), accompanied by a marked rise in nitrate concentration (from 4.21 to 5.14 $\mu g\cdot m^{-3}$; Fig. 6d). Correspondingly, N_{ait}

https://doi.org/10.5194/egusphere-2025-6512
Preprint. Discussion started: 5 February 2026

showed a recovery trend from 7–9 h. Overall, winter NPF was characterized by low FR and GR, dominated by primary emissions. The high abundance of primary pollutants diluted overall aerosol hygroscopicity, yielding the lowest seasonal κ (0.08) and consequently reducing the CCN activation efficiency of newly formed particles.

3.4 Particle growth controls CCN formation from NPF events

In summer, although NPF frequency was the lowest, it had a significant enhancing effect on N_{CCN}. E_N_{CCN} at 0.4 % SS was as high as 1.64 (Fig. 7a). In the initial stage of NPF events (0–2 hours), N_{CCN} showed a sharp decline. At 0.4 % SS, it decreased from about 2078 cm^{-3} to 1187 cm^{-3} (Fig. S12b). However, after 2 h, N_{CCN} recovered noticeably and later returned to or even exceeded initial levels. The CCN size distribution (Fig. 7c) showed that during the event, smaller CCN (1–3 μm) decreased, while CCN of 5.5–6.5 μm increased. For instance, CCN at 6 μm increased from 2607.7 to 3147.8 cm^{-3}. Summer NPF promoted CCN growth to larger sizes. However, the daily average N_{CCN} on summer NPF days was lower than on non-NPF days, possibly due to the extremely low NPF frequency (4.35 %) and the sharp decline in CCN at the beginning of events, affecting the daily average.

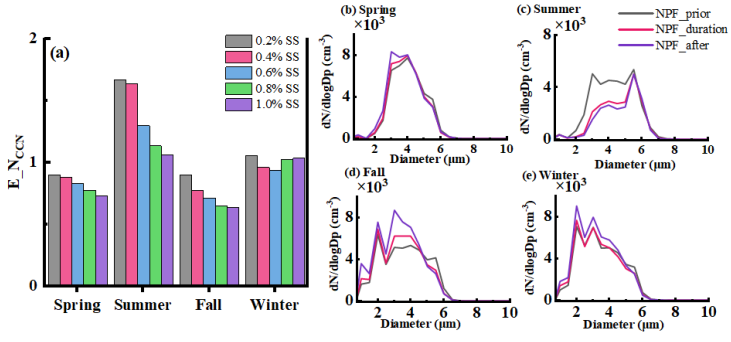

Fig. 7 The contribution of NPF events to cloud condensation nuclei (CCN) across seasons: (a) CCN enhancement (E_N_{CCN}), and (b-e) particle number size distributions at 2 hours before, during, and 5 hours after the NPF event for seasons.

Spring NPF events' impact on N_{CCN} showed significant suppression. Throughout the event, N_{CCN} at various supersaturation levels showed only weak and slow increases. N_{CCN} (0.4 % SS, the same as below) increased from a pre-event average (-4 to -1 h) of about 2636 cm^{-3} to 3192 cm^{-3} at 4 h, then rapidly declined (Fig. S12c). E_N_{CCN} at 0.4 % SS was only 0.88. This phenomenon corresponds to the "high

https://doi.org/10.5194/egusphere-2025-6512
Preprint. Discussion started: 5 February 2026

formation, suppressed growth" characteristic of spring NPF. Despite the explosive generation of nucleation-mode particles, severe competition under high CS severely hindered subsequent growth of new particles, preventing them from effectively growing to CCN activation sizes, resulting in a weak or even negative contribution to CCN.

In fall events, from 2 h onward, N_{CCN} began to increase, rising from 3471 cm^{-3} to a maximum of 4752 cm^{-3}, forming a high-value plateau lasting from 3 h to 8 h (Fig. S12d). After the NPF event, N_{CCN} increased significantly across the 1-5 μm size range (Fig. 7d). Fall NPF events most effectively and broadly increased the number of particles available for cloud droplet activation in the atmosphere. Although E_N_{CCN} was lower due to the modest initial stage, the post-event enhancement effect was significant. This evolution process is consistent with the sustained particle growth process in fall NPF, allowing new particles to grow steadily to CCN activation sizes.

In winter NPF events, N_{CCN} was low in the early stage (0–4 h), with insignificant growth. However, from 5 h onward, N_{CCN} growth became significant, increasing from 4483 cm^{-3} to 6173 cm^{-3} and remaining stable at high levels (Fig. S12d). During the event, changes in the CCN size distribution were not obvious. However, after the NPF event, CCN in the 2–5 μm size range showed the most significant growth (e.g., at 2 μm, from 7073.0 to 9045.1 cm^{-3}; Fig. 7e).

4 Conclusions

This year-long observational study in coastal Fuzhou revealed distinct seasonal patterns in new particle formation (NPF) and its impact on cloud condensation nuclei (CCN). We identified 46 NPF events, which predominantly occurred between 09:00 and 12:00. Key quantitative results include: the highest seasonal formation rate (FR) in spring (5.56 cm^{-3} s^{-1}), the highest growth rate (GR) in summer (peak at 11.68 nm h^{-1}), and the strongest CCN enhancement in summer (E_N_{CCN} = 1.64 at 0.4 % SS). In fall and winter, CCN increases (13–65 %) lag NPF events by 3–5 h.

A total of 46 NPF events occurred during the observation period, with a frequency of 12.7 %. NPF event start times were mainly concentrated between 08:00 and 13:00 (accounting for 85 % of all events), with an average duration of 4 h. The annual averages for formation rate (FR), growth rate (GR), condensation

https://doi.org/10.5194/egusphere-2025-6512
Preprint. Discussion started: 5 February 2026

sink (CS), coagulation sink (CoagS), and condensable vapor concentration (C) were 3.94 ± 8.26 $cm^{-3}·s^{-1}$, 5.20 ± 1.78 $nm·h^{-1}$, $4.2×10^{-2}$ s^{-1}, $5.6×10^{-4}$ s^{-1}, and $16.7×10^{7}$ cm^{-3}, respectively.

The seasonal contrast is mechanistically driven by the interplay between precursor availability, condensation sink (CS), and aerosol chemistry. Spring conditions favor high FR due to strong photochemistry and abundant precursors, but high CS suppresses subsequent growth. In summer, a low CS environment allows newly formed particles to grow efficiently, maximizing their contribution to CCN. The chemical composition shifts from sulfate- and nitrate-dominated in spring and summer ($\kappa >$ 0.1) to carbonaceous-aerosol-dominated in fall and winter ($\kappa \approx 0.09$), directly modulating particle hygroscopicity and CCN activation potential.

This study is based on a single year of data at an urban coastal site. The conclusions, particularly regarding inter-annual variability and the representativeness of the identified seasonal patterns, would benefit from longer-term observations. Furthermore, while online composition measurements provided valuable insights, more detailed speciated volatile organic compound (VOC) data would help constrain the precise roles of organic precursors in nucleation and growth across seasons.

This work demonstrates that the climatic impact of NPF in coastal urban areas is not simply a function of its occurrence frequency or formation strength. Instead, it is seasonally modulated by a competition between formation and growth-sink processes, and by the resulting aerosol chemical composition. The decoupling of high FR from effective CCN production (as in spring) implies that climate models using NPF frequency as a proxy for aerosol indirect effects may overestimate the impact in high-CS coastal regions. Conversely, the efficient growth and CCN enhancement in summer suggest that even infrequent NPF events can substantially influence cloud properties in such environments. These insights are crucial for developing more accurate parameterizations of aerosol-cloud-climate interactions in rapidly developing coastal zones.

Data availability

Data will be made available on request.

https://doi.org/10.5194/egusphere-2025-6512
Preprint. Discussion started: 5 February 2026

Author contributions

Conceptualization was completed by ZW and HW. Formal analysis and software modification were carried out by ZW and HW. The initial draft was written by ZW, incorporating tables provided by HW. The first draft was revised by ZW, HW, and YB, with input from HW, YB, FZ, WL, JH, LS, and ZX; subsequent versions of the manuscript were reviewed and edited by all authors. Data curation and collection were conducted by all authors. Funding acquisition was secured by HW.

Competing interests

The authors declare that they have no conflict of interest.

Disclaimer

Copernicus Publications remains neutral with regard to jurisdictional claims made in the text, published maps, institutional affiliations, or any other geographical representation in this paper. While Copernicus Publications makes every effort to include appropriate place names, the final responsibility lies with the authors. Views expressed in the text are those of the authors and do not necessarily reflect the views of the publisher.

Acknowledgements

The authors are grateful for the assistance with sample collection. We would like to thank the China National Environmental Monitoring Centre's real-time urban air quality release platform (http://106.37.208.233:20035/)

Financial support

This study was supported by the National Key Research and Development Program of China (Grant No., 2022YFC3701204), the National Natural Science Foundation of China (42505181 and U22A20578), Natural Science Foundation of Fujian Province, China (2024J01168 and 2023R1014003), the Natural Science Foundation of Jiangsu Province (BK20231300), and the Open Fund of Fujian Key Laboratory of Severe Weather and Key Laboratory of Straits Severe Weather (2024KFKT05).

https://doi.org/10.5194/egusphere-2025-6512
Preprint. Discussion started: 5 February 2026

References

Cai, M., Tan, H., Chan, C. K., Qin, Y., Xu, H., Li, F., Schurman, M. I., Liu, L., and Zhao, J.: The size-resolved cloud condensation nuclei (CCN) activity and its prediction based on aerosol hygroscopicity and composition in the pearl delta river (PRD) region during wintertime 2014, Atmos. Chem. Phys., 18, 16419–16437, https://doi.org/10.5194/acp-18-16419-2018, 2018.

Chang, Y., Deng, C., Cao, F., Cao, C., Zou, Z., Liu, S., Lee, X., Li, J., Zhang, G., and Zhang, Y.: Assessment of carbonaceous aerosols in Shanghai, China–Part 1: long-term evolution, seasonal variations, and meteorological effects, Atmos. Chem. Phys., 17, 9945–9964, https://doi.org/10.5194/acp-17-9945-2017, 2017.

Chen, M., Titcombe, M., Jiang, J., Jen, C., Kuang, C., Fischer, M. L., Eisele, F. L., Siepmann, J. I., Hanson, D. R., Zhao, J., and McMurry, P. H.: Acid–base chemical reaction model for nucleation rates in the polluted atmospheric boundary layer, Proc. Natl. Acad. Sci., 109, 18713–18718, https://doi.org/10.1073/pnas.1210285109, 2012.

Chen, Y., Wang, X., Dai, W., Wang, Q., Guo, X., Liu, Y., Qi, W., Shen, M., Zhang, Y., Li, L., Cao, Y., Wang, Y., and Li, J.: Particle Number Size Distribution of Wintertime Alpine Aerosols and Their Activation as Cloud Condensation Nuclei in the Guanzhong Plain, Northwest China, J. Geophys. Res.: Atmos., 128, e2022JD037877, https://doi.org/10.1029/2022JD037877, 2023.

Dusek, U., Frank, G. P., Curtius, J., Drewnick, F., Schneider, J., Kürten, A., Rose, D., Andreae, M. O., Borrmann, S., and Pöschl, U.: Enhanced organic mass fraction and decreased hygroscopicity of cloud condensation nuclei (CCN) during new particle formation events, https://doi.org/10.1029/2009GL040930, n.d.

Fan, J., Rosenfeld, D., Zhang, Y., Giangrande, S. E., Li, Z., Machado, L. A. T., Martin, S. T., Yang, Y., Wang, J., Artaxo, P., Barbosa, H. M. J., Braga, R. C., Comstock, J. M., Feng, Z., Gao, W., Gomes, H. B., Mei, F., Pöhlker, C., Pöhlker, M. L., Pöschl, U., and de Souza, R. A. F.: Substantial convection and precipitation enhancements by ultrafine aerosol particles, Science, 359, 411–418, https://doi.org/10.1126/science.aan8461, 2018.

https://doi.org/10.5194/egusphere-2025-6512
Preprint. Discussion started: 5 February 2026

453 Guo, S., Hu, M., Zamora, M. L., Peng, J., Shang, D., Zheng, J., Du, Z., Wu, Z., Shao, M., Zeng, L.,
454 Molina, M. J., and Zhang, R.: Elucidating severe urban haze formation in China, Proc. Natl. Acad. Sci.,
455 111, 17373–17378, https://doi.org/10.1073/pnas.1419604111, 2014.
456 Heintzenberg, J., Wehner, B., and Birmili, W.: 'How to find bananas in the atmospheric aerosol': new
457 approach for analyzing atmospheric nucleation and growth events, Tellus B, 59, 273–282,
458 https://doi.org/10.1111/j.1600-0889.2007.00249.x, 2007.
459 Hirsikko, A., Nieminen, T., Gagné, S., Lehtipalo, K., Manninen, H. E., Ehn, M., Hõrrak, U., Kerminen,
460 V.-M., Laakso, L., McMurry, P. H., Mirme, A., Mirme, S., Petäjä, T., Tammet, H., Vakkari, V., Vana,
461 M., and Kulmala, M.: Atmospheric ions and nucleation: a review of observations, Atmos. Chem. Phys.,
462 11, 767–798, https://doi.org/10.5194/acp-11-767-2011, 2011.
463 Hu, J., Shi, C., Ni, E., Liu, J., Zhai, S., Zhao, T., Jiang, B., Jiang, D., Wang, H., and Huang, Q.:
464 Recirculated transport mechanism aggravates ozone pollution over the mountainous coastal region:
465 Increased contribution from vertical mixing, Atmos. Environ., 332, 120617,
466 https://doi.org/10.1016/j.atmosenv.2024.120617, 2024.
467 Jayaratne, R., Pushpawela, B., He, C., Li, H., Gao, J., Chai, F., and Morawska, L.: Observations of
468 particles at their formation sizes in beijing, china, Atmos. Chem. Phys., 17, 8825–8835,
469 https://doi.org/10.5194/acp-17-8825-2017, 2017.
470 Jokinen, T., Sipilä, M., Kontkanen, J., Vakkari, V., Tisler, P., Duplissy, E.-M., Junninen, H.,
471 Kangasluoma, J., Manninen, H. E., Petäjä, T., Kulmala, M., Worsnop, D. R., Kirkby, J., Virkkula, A.,
472 and Kerminen, V.-M.: Ion-induced sulfuric acid–ammonia nucleation drives particle formation in coastal
473 antarctica, Sci. Adv., https://doi.org/10.1126/sciadv.aat9744, 2018.
474 Kawana, K., Miyazaki, Y., Omori, Y., Tanimoto, H., Kagami, S., Suzuki, K., Yamashita, Y., Nishioka,
475 J., Deng, Y., Yai, H., and Mochida, M.: Number-Size Distribution and CCN Activity of Atmospheric
476 Aerosols in the Western North Pacific During Spring Pre-Bloom Period: Influences of Terrestrial and
477 Marine Sources, J. Geophys. Res.: Atmos., 127, e2022JD036690, https://doi.org/10.1029/2022JD036690,
478 2022.

https://doi.org/10.5194/egusphere-2025-6512
Preprint. Discussion started: 5 February 2026

Kirchstetter, T. W., Novakov, T., and Hobbs, P. V.: Evidence that the spectral dependence of light absorption by aerosols is affected by organic carbon, J. Geophys. Res.: Atmos., 109, 2004JD004999, https://doi.org/10.1029/2004JD004999, 2004.

Kirkby, J., Duplissy, J., Sengupta, K., Frege, C., Gordon, H., Williamson, C., Heinritzi, M., Simon, M., Yan, C., Almeida, J., Tröstl, J., Nieminen, T., Ortega, I. K., Wagner, R., Adamov, A., Amorim, A., Bernhammer, A.-K., Bianchi, F., Breitenlechner, M., Brilke, S., Chen, X., Craven, J., Dias, A., Ehrhart, S., Flagan, R. C., Franchin, A., Fuchs, C., Guida, R., Hakala, J., Hoyle, C. R., Jokinen, T., Junninen, H., Kangasluoma, J., Kim, J., Krapf, M., Kürten, A., Laaksonen, A., Lehtipalo, K., Makhmutov, V., Mathot, S., Molteni, U., Onnela, A., Peräkylä, O., Piel, F., Petäjä, T., Praplan, A. P., Pringle, K., Rap, A., Richards, N. A. D., Riipinen, I., Rissanen, M. P., Rondo, L., Sarnela, N., Schobesberger, S., Scott, C. E., Seinfeld, J. H., Sipilä, M., Steiner, G., Stozhkov, Y., Stratmann, F., Tomé, A., Virtanen, A., Vogel, A. L., Wagner, A. C., Wagner, P. E., Weingartner, E., Wimmer, D., Winkler, P. M., Ye, P., Zhang, X., Hansel, A., Dommen, J., Donahue, N. M., Worsnop, D. R., Baltensperger, U., Kulmala, M., Carslaw, K. S., and Curtius, J.: Ion-induced nucleation of pure biogenic particles, Nature, 533, 521–526, https://doi.org/10.1038/nature17953, 2016.

Kulmala, M., Vehkamäki, H., Petäjä, T., Dal Maso, M., Lauri, A., Kerminen, V.-M., Birmili, W., and McMurry, P. H.: Formation and growth rates of ultrafine atmospheric particles: a review of observations, J. Aerosol Sci., 35, 143–176, https://doi.org/10.1016/j.jaerosci.2003.10.003, 2004.

Kulmala, M., Petäjä, T., Nieminen, T., Sipilä, M., Manninen, H. E., Lehtipalo, K., Dal Maso, M., Aalto, P. P., Junninen, H., Paasonen, P., Riipinen, I., Lehtinen, K. E. J., Laaksonen, A., and Kerminen, V.-M.: Measurement of the nucleation of atmospheric aerosol particles, Nat. Protoc., 7, 1651–1667, https://doi.org/10.1038/nprot.2012.091, 2012.

Kulmala, M., Dada, L., Daellenbach, K. R., Yan, C., Stolzenburg, D., Kontkanen, J., Ezhova, E., Hakala, S., Tuovinen, S., Kokkonen, T. V., Kurppa, M., Cai, R., Zhou, Y., Yin, R., Baalbaki, R., Chan, T., Chu, B., Deng, C., Fu, Y., Ge, M., He, H., Heikkinen, L., Junninen, H., Liu, Y., Lu, Y., Nie, W., Rusanen, A., Vakkari, V., Wang, Y., Yang, G., Yao, L., Zheng, J., Kujansuu, J., Kangasluoma, J., Petäjä, T., Paasonen, P., Järvi, L., Worsnop, D., Ding, A., Liu, Y., Wang, L., Jiang, J., Bianchi, F., and Kerminen, V.-M.: Is

https://doi.org/10.5194/egusphere-2025-6512
Preprint. Discussion started: 5 February 2026

506 reducing new particle formation a plausible solution to mitigate particulate air pollution in beijing and
507 other chinese megacities?, Faraday Discuss., 226, 334–347, https://doi.org/10.1039/D0FD00078G, 2021.
508 Kuwata, M., Kondo, Y., Miyazaki, Y., Komazaki, Y., Kim, J. H., Yum, S. S., Tanimoto, H., and
509 Matsueda, H.: Cloud condensation nuclei activity at Jeju Island, Korea in spring 2005, Atmos. Chem.
510 Phys., 8, 2933–2948, https://doi.org/10.5194/acp-8-2933-2008, 2008.
511 Lehtipalo, K., Yan, C., Dada, L., Bianchi, F., Xiao, M., Wagner, R., Stolzenburg, D., Ahonen, L. R.,
512 Amorim, A., Baccarini, A., Bauer, P. S., Baumgartner, B., Bergen, A., Bernhammer, A.-K.,
513 Breitenlechner, M., Brilke, S., Buchholz, A., Mazon, S. B., Chen, D., Chen, X., Dias, A., Dommen, J.,
514 Draper, D. C., Duplissy, J., Ehn, M., Finkenzeller, H., Fischer, L., Frege, C., Fuchs, C., Garmash, O.,
515 Gordon, H., Hakala, J., He, X., Heikkinen, L., Heinritzi, M., Helm, J. C., Hofbauer, V., Hoyle, C. R.,
516 Jokinen, T., Kangasluoma, J., Kerminen, V.-M., Kim, C., Kirkby, J., Kontkanen, J., Kürten, A., Lawler,
517 M. J., Mai, H., Mathot, S., MauldinIII, R. L., Molteni, U., Nichman, L., Nie, W., Nieminen, T., Ojdanic,
518 A., Onnela, A., Passananti, M., Petäjä, T., Piel, F., Pospisilova, V., Quéléver, L. L. J., Rissanen, M. P.,
519 Rose, C., Sarnela, N., Schallhart, S., Schuchmann, S., Sengupta, K., Simon, M., Sipilä, M., Tauber, C.,
520 Tomé, A., Tröstl, J., Väisänen, O., Vogel, A. L., Volkamer, R., Wagner, A. C., Wang, M., Weitz, L.,
521 Wimmer, D., Ye, P., Ylisirniö, A., Zha, Q., Carslaw, K. S., Curtius, J., Donahue, N. M., Flagan, R. C.,
522 Hansel, A., Riipinen, I., Virtanen, A., Winkler, P. M., Baltensperger, U., Kulmala, M., and Worsnop, D.
523 R.: Multicomponent new particle formation from sulfuric acid, ammonia, and biogenic vapors, Sci. Adv.,
524 https://doi.org/10.1126/sciadv.aau5363, 2018.
525 Leng, C., Zhang, Q., Tao, J., Zhang, H., Zhang, D., Xu, C., Li, X., Kong, L., Cheng, T., Zhang, R., Yang,
526 X., Chen, J., Qiao, L., Lou, S., Wang, H., and Chen, C.: Impacts of new particle formation on aerosol
527 cloud condensation nuclei (CCN) activity in shanghai: case study, Atmos. Chem. Phys., 14, 11353–
528 11365, https://doi.org/10.5194/acp-14-11353-2014, 2014.
529 Lv, G., Sui, X., Chen, J., Jayaratne, R., and Mellouki, A.: Investigation of new particle formation at the
530 summit of Mt. Tai, China, Atmos. Chem. Phys., 18, 2243–2258, https://doi.org/10.5194/acp-18-2243-
531 2018, 2018.

https://doi.org/10.5194/egusphere-2025-6512
Preprint. Discussion started: 5 February 2026

532 Maso, M. D., Kulmala, M., Riipinen, I., Wagner, R., Hussein, T., Aalto, P., and Lehtinen, K.: Formation
533 and growth of fresh atmospheric aerosols: eight years of aerosol size distribution data from SMEAR II,
534 hyytiälä, Finland, Boreal Environ. Res., 2005.
535 McMurry, P. H. and Friedlander, S. K.: New particle formation in the presence of an aerosol, Atmos.
536 Environ. (1967), 13, 1635–1651, https://doi.org/10.1016/0004-6981(79)90322-6, 1979.
537 Petters, M. D. and Kreidenweis, S. M.: A single parameter representation of hygroscopic growth and
538 cloud condensation nucleus activity, Atmos. Chem. Phys., 7, 1961–1971, https://doi.org/10.5194/acp-7-
539 1961-2007, 2007.
540 Ren, J., Chen, L., Fan, T., Liu, J., Jiang, S., and Zhang, F.: The NPF Effect on CCN Number
541 Concentrations: A Review and Re-Evaluation of Observations From 35 Sites Worldwide, Geophys. Res.
542 Lett., 48, e2021GL095190, https://doi.org/10.1029/2021GL095190, 2021.
543 Rose, C., Sellegri, K., Moreno, I., Velarde, F., Ramonet, M., Weinhold, K., Krejci, R., Andrade, M.,
544 Wiedensohler, A., Ginot, P., and Laj, P.: CCN production by new particle formation in the free
545 troposphere, Atmos. Chem. Phys., 17, 1529–1541, https://doi.org/10.5194/acp-17-1529-2017, 2017.
546 Rose, D., Gunthe, S. S., Mikhailov, E., Frank, G. P., Dusek, U., Andreae, M. O., and Pöschl, U.:
547 Calibration and measurement uncertainties of a continuous-flow cloud condensation nuclei counter
548 (DMT-CCNC): CCN activation of ammonium sulfate and sodium chloride aerosol particles in theory
549 and experiment, Atmos. Chem. Phys., 8, 1153–1179, https://doi.org/10.5194/acp-8-1153-2008, 2008.
550 Shen, X., Sun, J., Kivekäs, N., Kristensson, A., Zhang, X., Zhang, Y., Zhang, L., Fan, R., Qi, X., Ma, Q.,
551 and Zhou, H.: Spatial distribution and occurrence probability of regional new particle formation events
552 in eastern China, Atmos. Chem. Phys., 18, 587 – 599, https://doi.org/10.5194/acp-18-587-2018, 2018.
553 Sun, Y. L., Wang, Z. F., Du, W., Zhang, Q., Wang, Q. Q., Fu, P. Q., Pan, X. L., Li, J., Jayne, J., and
554 Worsnop, D. R.: Long-term real-time measurements of aerosol particle composition in beijing, china:
555 seasonal variations, meteorological effects, and source analysis, Atmos. Chem. Phys., 15, 10149–10165,
556 https://doi.org/10.5194/acp-15-10149-2015, 2015.
557 Tröstl, J., Chuang, W. K., Gordon, H., Heinritzi, M., Yan, C., Molteni, U., Ahlm, L., Frege, C., Bianchi,
558 F., Wagner, R., Simon, M., Lehtipalo, K., Williamson, C., Craven, J. S., Duplissy, J., Adamov, A.,
559 Almeida, J., Bernhammer, A.-K., Breitenlechner, M., Brilke, S., Dias, A., Ehrhart, S., Flagan, R. C.,

https://doi.org/10.5194/egusphere-2025-6512
Preprint. Discussion started: 5 February 2026

Franchin, A., Fuchs, C., Guida, R., Gysel, M., Hansel, A., Hoyle, C. R., Jokinen, T., Junninen, H., Kangasluoma, J., Keskinen, H., Kim, J., Krapf, M., Kürten, A., Laaksonen, A., Lawler, M., Leiminger, M., Mathot, S., Möhler, O., Nieminen, T., Onnela, A., Petäjä, T., Piel, F. M., Miettinen, P., Rissanen, M. P., Rondo, L., Sarnela, N., Schobesberger, S., Sengupta, K., Sipilä, M., Smith, J. N., Steiner, G., Tomè, A., Virtanen, A., Wagner, A. C., Weingartner, E., Wimmer, D., Winkler, P. M., Ye, P., Carslaw, K. S., Curtius, J., Dommen, J., Kirkby, J., Kulmala, M., Riipinen, I., Worsnop, D. R., Donahue, N. M., and Baltensperger, U.: The role of low-volatility organic compounds in initial particle growth in the atmosphere, Nature, 533, 527–531, https://doi.org/10.1038/nature18271, 2016.

Wang, H., Zhu, B., Shen, L., An, J., Yin, Y., and Kang, H.: Number size distribution of aerosols at Mt. Huang and nanjing in the Yangtze River delta, china: effects of air masses and characteristics of new particle formation, Atmos. Res., 150, 42–56, https://doi.org/10.1016/j.atmosres.2014.07.020, 2014.

Wang, Z. B., Hu, M., Yue, D. L., Zheng, J., Zhang, R. Y., Wiedensohler, A., Wu, Z. J., Nieminen, T., and Boy, M.: Evaluation on the role of sulfuric acid in the mechanisms of new particle formation for beijing case, Atmos. Chem. Phys., 11, 12663–12671, https://doi.org/10.5194/acp-11-12663-2011, 2011.

Wildt, J., Mentel, T. F., Kiendler-Scharr, A., Hoffmann, T., Andres, S., Ehn, M., Kleist, E., Müsgen, P., Rohrer, F., Rudich, Y., Springer, M., Tillmann, R., and Wahner, A.: Suppression of new particle formation from monoterpene oxidation by NOx, Atmos. Chem. Phys., 14, 2789–2804, https://doi.org/10.5194/acp-14-2789-2014, 2014.

Williamson, C. J., Kupc, A., Axisa, D., Bilsback, K. R., Bui, T., Campuzano-Jost, P., Dollner, M., Froyd, K. D., Hodshire, A. L., Jimenez, J. L., Kodros, J. K., Luo, G., Murphy, D. M., Nault, B. A., Ray, E. A., Weinzierl, B., Wilson, J. C., Yu, F., Yu, P., Pierce, J. R., and Brock, C. A.: A large source of cloud condensation nuclei from new particle formation in the tropics, Nature, 574, 399–403, https://doi.org/10.1038/s41586-019-1638-9, 2019.

Wu, C. and Yu, J. Z.: Determination of primary combustion source organic carbon-to-elemental carbon (OC / EC) ratio using ambient OC and EC measurements: secondary OC-EC correlation minimization method, Atmos. Chem. Phys., 16, 5453–5465, https://doi.org/10.5194/acp-16-5453-2016, 2016.

https://doi.org/10.5194/egusphere-2025-6512
Preprint. Discussion started: 5 February 2026

586 Xiao, S., Wang, M. Y., Yao, L., Kulmala, M., Zhou, B., Yang, X., Chen, J. M., Wang, D. F., Fu, Q. Y.,
587 Worsnop, D. R., and Wang, L.: Strong atmospheric new particle formation in winter in urban shanghai,
588 china, Atmos. Chem. Phys., 15, 1769–1781, https://doi.org/10.5194/acp-15-1769-2015, 2015.
589 Xu, W., Ovadnevaite, J., Fossum, K. N., Lin, C., Huang, R.-J., O'Dowd, C., and Ceburnis, D.: Aerosol
590 hygroscopicity and its link to chemical composition in the coastal atmosphere of Mace Head: marine and
591 continental air masses, Atmos. Chem. Phys., 20, 3777–3791, https://doi.org/10.5194/acp-20-3777-2020,
592 2020.
593 Yao, L., Garmash, O., Bianchi, F., Zheng, J., Yan, C., Kontkanen, J., Junninen, H., Mazon, S. B., Ehn,
594 M., Paasonen, P., Sipilä, M., Wang, M., Wang, X., Xiao, S., Chen, H., Lu, Y., Zhang, B., Wang, D., Fu,
595 Q., Geng, F., Li, L., Wang, H., Qiao, L., Yang, X., Chen, J., Kerminen, V.-M., Petäjä, T., Worsnop, D.
596 R., Kulmala, M., and Wang, L.: Atmospheric new particle formation from sulfuric acid and amines in a
597 chinese megacity, Science, https://doi.org/10.1126/science.aao4839, 2018.
598 Yli-Juuti, T., Nieminen, T., Hirsikko, A., Aalto, P. P., Asmi, E., Hõrrak, U., Manninen, H. E., Patokoski,
599 J., Dal Maso, M., Petäjä, T., Rinne, J., Kulmala, M., and Riipinen, I.: Growth rates of nucleation mode
600 particles in hyytiälä during 2003&minus- 2009: variation with particle size, season, data analysis method
601 and ambient conditions, Atmos. Chem. Phys., 11, 12865–12886, https://doi.org/10.5194/acp-11-12865-
602 2011, 2011.
603 Yue, D. L., Hu, M., Zhang, R. Y., Wu, Z. J., Su, H., Wang, Z. B., Peng, J. F., He, L. Y., Huang, X. F.,
604 Gong, Y. G., and Wiedensohler, A.: Potential contribution of new particle formation to cloud
605 condensation nuclei in Beijing, Atmos. Environ., 45, 6070–6077,
606 https://doi.org/10.1016/j.atmosenv.2011.07.037, 2011.
607 Zaveri, R. A., Wang, J., Fan, J., Zhang, Y., Shilling, J. E., Zelenyuk, A., Mei, F., Newsom, R., Pekour,
608 M., Tomlinson, J., Comstock, J. M., Shrivastava, M., Fortner, E., Machado, L. A. T., Artaxo, P., and
609 Martin, S. T.: Rapid growth of anthropogenic organic nanoparticles greatly alters cloud life cycle in the
610 Amazon rainforest, Science Advances, 8, eabj0329, https://doi.org/10.1126/sciadv.abj0329, 2022.
611